International Journal of Ambient Energy

ISSN: (Print) (Online) Journal homepage: https://www.tandfonline.com/loi/taen20

Thermo-diffusion, chemical reaction, Hall and ion slip effects on MHD rotating flow of micro-polar fluid past an infinite vertical porous surface

M. Veera Krishna & Ali J. Chamkha

To cite this article: M. Veera Krishna & Ali J. Chamkha (2022) Thermo-diffusion, chemical reaction, Hall and ion slip effects on MHD rotating flow of micro-polar fluid past an infinite vertical porous surface, International Journal of Ambient Energy, 43:1, 5344-5356, DOI: 10.1080/01430750.2021.1946146

To link to this article: https://doi.org/10.1080/01430750.2021.1946146

Published online: 05 Jul 2021.

INTERNATIONAL JOURNAL OF AMBIENT ENERGY
2022, VOL. 43, NO. 1, 5344–5356
https://doi.org/10.1080/01430750.2021.1946146

Taylor & Francis
Taylor & Francis Group

Thermo-diffusion, chemical reaction, Hall and ion slip effects on MHD rotating flow of micro-polar fluid past an infinite vertical porous surface

M. Veera Krishna [a] and Ali J. Chamkha[b]

[a]Department of Mathematics, Rayalaseema University, Kurnool, India; [b]Faculty of Engineering, Kuwait College of Science and Technology, Safat, Kuwait

ABSTRACT

The current study explores the consequences of thermo-diffusion, chemical reaction, Hall and ion-slip impacts on unsteady heat and mass transport of free convective hydro-magnetic micro-polar liquid flow enclosed in a semi-infinite porous plate within a gyratory frame with transverse magnetic field and convective boundary conditions. The non-dimensional governing equations are systematically solved by means of the finite element method. Using graphical profiles, the outcomes of a variety of significant parameters within the boundary layer are addressed. Additionally, the local skin friction coefficient and rates of heat and mass transports in expressions of the local Nusselt number and local Sherwood number are presented digitally in a tabular form, and it was found that the Nusselt number and Sherwood number remain constant with all the varying pertinent parameters.

ARTICLE HISTORY
Received 30 January 2020
Accepted 16 June 2021

KEYWORDS
Micropolar fluid; suction; chemical reaction; finite element method; rotating frame

Nomenclature

u, v:	velocity components in (x, y)-directions (m s^{-1})
x, y:	Cartesian co-ordinates (m)
t:	time (s)
k:	permeability of porous medium (m^2)
j:	micro-inertia density (m^2)
g:	acceleration due to gravity (m s^{-2})
T:	temperature of the fluid (K)
T_∞:	free stream temperature (K)
T_w:	temperature at the wall (K)
q:	complex velocity $(u + iv)$ (m s^{-1})
k_1:	thermal conductivity of the fluid (W m^{-1} K^{-1})
q_r:	radiative heat flux (W m^{-2})
u_p:	uniform velocity of the plate in its own plane (m s^{-1})
C:	concentration of the fluid (mol m^{-3})
C_∞:	free stream concentration (mol m^{-3})
C_f:	skin friction coefficient
C_w:	wall shear stress (Pascal)
C'_ω:	local couple stress coefficient at the wall
C_p:	specific heat at constant pressure (J kg^{-1} K^{-1})
D_m:	molecular diffusivity (m^2 s^{-1})
K_T:	thermo diffusion ratio
U_r:	uniform reference velocity (m s^{-1})
ε:	smallest constant quantity
w_0:	normal velocity at the plate which is positive for suction and negative for blowing (m s^{-1})
k^*:	mean absorption coefficient (m^{-1})
Nu:	Nusselt number
Sh:	Sherwood number
n:	frequency of oscillation (Hz)
B:	magnetic field vector (A/m)
E:	external electric field (c)
J:	current density vector (A/m^2)
V:	velocity vector (m/s)
Kr:	first-order chemical reaction parameter
Q_0:	heat absorption coefficient
R:	rotation parameter
M:	magnetic field parameter
Pr:	Prandtl number
Sc:	Schmidt number
Gr:	thermal Grashof number
Gm:	mass Grashof number
N:	heat radiation parameter
K:	permeability parameter,
Du:	Dufour number,
S:	suction parameter,
Kc:	chemical reaction parameter
Q:	heat absorption parameter

Greek symbols

$\bar{\omega}_1$, $\bar{\omega}_2$:	micro-rotation components along the x and y-axis respectively
β_T, β_C:	coefficient of thermal expansion and concentration expansion
ρ:	density of the fluid
ν:	kinematic viscosity
ν_r:	kinematic micro-rotation viscosity
ω_e:	cyclotron frequency (e/mB)
τ_e:	electron collision time (s)
β_i:	ion slip parameter
β_e:	Hall parameter

CONTACT M. Veera Krishna veerakrishna_maths@yahoo.com

δ: dimensionless material parameter,
λ: the viscosity ratio
σ^*: Stefan–Boltzman constant
σ: electrical conductivity of the fluid
Λ: spin gradient velocity

Superscripts

e: electron
i: ion
w: wall
∞: free stream condition

1. Introduction

The theory of micro-polar fluids has received much attention in the last several years because the traditional Newtonian fluids cannot precisely describe the characteristics of fluid flow for a fluid with suspended particles. The micro-polar fluids may be described as non-Newtonian fluids consisting of dumb-bell molecules or short rigid cylindrical elements suspended in a viscous medium where the deformation of fluid particles is ignored. Some examples are polymer fluids, fluid suspensions, animal blood, etc. The presence of dust or smoke, particularly in a gas, may also be modelled using micro-polar fluid dynamics. Micro-polar fluids are fluids with a microstructure. They belong to a class of fluids with non-symmetric stress tensor which are termed as polar fluids, and include, as a special case, the well-established Navier–Stokes model of classical fluids which are termed as ordinary fluids.

A number of mathematical models have been proposed to explain the rheological behaviour of non-Newtonian fluids. Among these, a model which has been most widely used for non-Newtonian fluids, and is frequently encountered in chemical engineering processes, is the micro-fluid model. It has been successfully applied to non-Newtonian fluids experimentally. In modern decades, the investigation of heat and mass transfer through micro-polar fluids has been regarded comprehensively due to their assortment of industrial applications. The convective heat and mass transport through Newtonian and non-Newtonian fluids might be thoroughly utilised for polymer construction, these are fibre and granulated separation, geo-thermal regimes, wineglass-fibre and paper manufacture, refrigerating of metalised covers, geo-thermal repositories, thermal insulating material, strengthened oil rehabilitation, packing bed incentivised reactors, etc. Eringen's theory (Erigen 1996) has presented an outstanding model for acquiring knowledge for a number of confusing fluids, that is, highly dispersed fluids, polymeric fluids and blood. He has given importance to micro-polar fluid as it contains extended and renowned scope of exploration due to its implementation in several phenomena that are used in industry. Some examples include exotic lubricants, muddy fluids, liquid crystals, polymer blends polymeric fluids, real fluids by means of suspensions, liquid crystal, animal blood, aero gels, alloys, and micro emulsions, anisotropic fluids, rigid molecules, magnetic fluids and clouds with dust. Mishra et al. (2018) discussed the free convective flow of a micro-polar fluid over a shrinking sheet with heat source. Analytic approximate solutions for heat transfer of a micro-polar fluid through a porous medium with radiation effect have been studied by Rashidi, Mohimanian, and Abbasbandy (2011). Ziaul Haque et al. (2012) investigated the behaviour of micro-polar fluid on steady magneohydrodynamics (MHD) free convective and mass transfer flow with constant heat and mass fluxes, Joule heating and viscous dissipation. Free convective MHD micro-polar fluid flow with thermal radiation and radiation absorption has been studied numerically by Pradhan et al. (2019).

The study of thermal radiation in heterogeneous areas in engineering such as nuclear power plants, multifarious propulsion devices for missiles, liquid metal fluids, gas turbines and so forth, due to small coefficient of convective heat transfer, shows the presence of surface heat transfer. Thermal radiation is utilised in numerous applications because radiant emission relies on temperature. Biswas et al. (2019) investigated the unsteady MHD heat and mass transfer micro-polar fluid flow in the presence of radiation and chemical reaction through a vertical porous plate using explicit finite difference analysis. The MHD pulsating flow of the Casson fluid in a porous channel with thermal radiation and chemical reaction has been explored by Srinivas, Kumar, and Reddy (2018). Sobamowo (2018) studied the heat transfer effects of thermal radiation on free convection flow of Casson nanofluid over a vertical plate. The effects of chemical reaction and heat generation/absorption on MHD Casson fluid flow over an exponentially accelerated vertical plate embedded in a porous medium with ramped wall temperature and ramped surface concentration have been investigated by Hari and Harshad (2019). Ahmmed, Biswas, and Afikuzzaman (2018) have discussed the unsteady MHD free convection flow of nanofluid through an exponentially accelerated inclined plate embedded in a porous medium with variable thermal conductivity in the presence of radiation.

The gyratory liquids are extremely imperative. For this reason of its happening in an assortment of expected phenomenon as well as technological requirements through the Coriolis force. The literature has several examples of a number of momentous and several characteristics of rotational fluids. Coriolis force effect is an essential gelatinous and nonreactive force. Moreover, the strengths of magnetic and Coriolis are comparable but they have disadvantages. The Hall and ion-slip impacts include on the vector form with transitionally lying on the magnetic field strength idiom. Ellahi, Bhatti, and Pop (2016) discussed the Hall and ion-slip impacts on the peristalsis Jeffrey liquid stream through a rectangular channel which are inhomogeneous. Bhatti, Abbas, and Rashidi (2016) carried out research on the consequences of Hall and ion-slip on non-Newtonian fluid flow with the Reynolds number as zero. Srinivasacharya and Shafeeurrahman (2017) studied using two analogous concentric cylinders for the Hall and ion slip effects on MHD mixed convective nanofluid. Jitendra and Srinivasa (2018) explored Hall and ion slip consequences on convective flow of revolving fluid through a perpendicular expanding and accelerating surface. Krishna and Chamkha (2019) explored the heat radiation and heat absorption, diffusion-thermo and Hall and ion slip effects using MHD natural convection gyrating flow by nanofluids past a moving porous plate with constant heat source. Sara and Bhatti (2018) explored the MHD pumping flow of a

non-Newtonian nano-fluid using chemical reactions, and Hall and ion slip consequences. Krishna (2021) investigated the radiation absorption, chemical reaction, and Hall and ion slip impacts on MHD free convection flow past a semi-infinite moving porous surface. Krishna, Swarnalathamma, and Chamkha (2018) studied the heat and mass transport impacts on a variable flow of a chemical reactive micro-polar fluid past an unlimited perpendicular porous plate for the occurrence of a transverse magnetic field, Hall currents and heat radiation concept. Research was done on the heat and mass transport impacts on free convection flow of micro-polar fluid on an infinite vertical porous plate having transverse magnetic field through a constant suction velocity and captivating Hall impacts (Krishna, Anand, and Chamkha 2019). Krishna, Ahamad, and Chamkha (2020a) researched the Hall and ion slip impacts on the unsteady hydromagnetic natural convective gyrating flow through a porous medium over an exponential accelerated plate. The united effects of Hall and ion slip for MHD gyrating flow of ciliary propulsion of microscopic organisms through porous media were studied by Krishna, Sravanthi, and Gorla (2020b). Krishna and Chamkha (2020a) investigated the Hall and ion slip effects on the MHD convective flow of elastico-viscous fluid through a porous medium between two rigidly rotating parallel plates with time and fluctuating sinusoidal pressure gradient. Krishna (2020a) reported the Hall and ion slip effects on MHD free convective rotating flow bounded by the semi-infinite vertical porous surface. Krishna (2020b) discussed the MHD laminar flow of an elastico-viscous electrically conducting Walter's fluid through a circular cylinder or a pipe. The Hall and ion slip effects on unsteady MHD convective rotating flow of nanofluids have been discussed by Krishna and Chamkha (2020b). Pal and Biswas (2018) reported double diffusion temperature and mass transport features of an oscillating viscous electrically conducting micro-polar liquid through a moving plate utilising the convective boundary condition and chemical reaction effect. Nanofluid natural convection in a baffled U-shaped enclosure in the presence of a magnetic field has been investigated by Ma et al. (2018). Bhatti et al. (2018) examined three-dimensional unsteady MHD boundary layer flow of viscous nanofluid having gyrotactic microorganisms through a stretching porous cylinder. Rashad et al. (2017) investigated the effect of magnetic field and internal heat generation on the free convection flow in a rectangular cavity. Here the cavity is filled with a porous medium saturated with Cu–water nanofluid. The effects of thermal radiation and rotation on the unsteady MHD convective flow past an infinite vertical moving absorbent plate have been investigated by Krishna, Ahamad, and Chamkha (2021a). Krishna, Ahamad, and Chamkha (2021b) discussed the radiation absorption on MHD convective flow of nanofluids through a perpendicularly travelling permeable plate.

Considering the above-mentioned facts, the consequences of thermo-diffusion, chemical reaction, Hall and ion-slip impacts lying on unsteady heat and mass transport of natural convective MHD micro-polar liquid flow enclosed past a semi-infinite porous plate within a gyratory frame under the accomplishment of a transverse magnetic field and convective boundary conditions are explored. The non-dimensional governing equations are solved systematically by means of the finite element method.

2. Formulation and solution of the problem

The consequences of thermo-diffusion, chemical reaction, Hall and ion-slip impacts lying on double diffusive heat and mass transport on unsteady free convective hydro-magnetic micro-polar fluid flow enclosed through a semi-infinite porous plate within a gyratory frame under the influence of transverse magnetic field and convective boundary conditions are explored. The assumptions are made as follows.

The movement of the flow is impinged by a uniform transverse magnetic field B_0 with the occurrence of thermal and concentration buoyancy forces. In the initial undisturbed state both the fluid and the plate are in rigid rotation with the same angular velocity Ω about the normal to the plate. The x-axis is considered along the plate in the upward direction as well as the z-axis is at right angles to it as revealed in Figure 1 (Krishna, Ahamad, and Aljohani 2021c). Induced magnetic field is negligible in comparison to the applied magnetic field. It is assumed that the magnetic field is of low intensity. Electric dissipation is neglected hence Joule heating is negligible. The fluid is considered to be grey absorbing or emitting radiation but not scattering medium. The Rosseland approximation is utilised to portray the radiative heat flux in the z-direction. The plate travels unremittingly with uniform velocity u_p in its own plane. It is assumed that the temperature of the surface should be held uniform at T_w, whereas those of the ambient temperature acquires the unvarying value T_∞, so that $T_w > T_\infty$. The concentration of the surface needs to be taken as C_w and that of the ambient fluid is taken as C_∞.

Under these assumptions, the boundary layer equations of motion, energy and mass-diffusion under the influence of uniform transverse magnetic field by the incidence of thermal diffusion and chemical reaction are as follows.

The governing equations of the flow are (Pal and Biswas 2018)

$$\frac{\partial w}{\partial z} = 0 \tag{1}$$

$$\frac{\partial u}{\partial t} + w\frac{\partial u}{\partial z} - 2\Omega v = (\nu + \nu_r)\frac{\partial^2 u}{\partial z^2} + \frac{B_0 J_y}{\rho} - \frac{\nu}{k}u + g\beta_T(T - T_\infty) + g\beta_C(C - C_\infty)$$

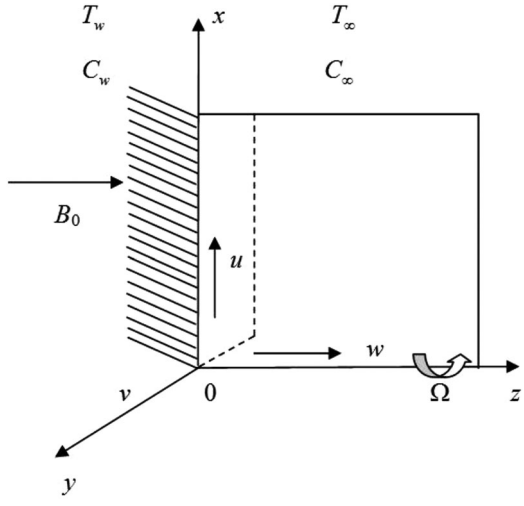

Figure 1. Physical model.

$$- \nu_r \frac{\partial \bar{\omega}_2}{\partial z} \tag{2}$$

$$\frac{\partial v}{\partial t} + w\frac{\partial v}{\partial z} + 2\Omega u = (\nu + \nu_r)\frac{\partial^2 v}{\partial z^2} - \frac{B_0 J_x}{\rho} - \frac{\nu}{k}v + \nu_r \frac{\partial \bar{\omega}_1}{\partial z} \tag{3}$$

$$\frac{\partial \bar{\omega}_1}{\partial t} + w\frac{\partial \bar{\omega}_1}{\partial z} = \frac{\Lambda}{\rho j}\frac{\partial^2 \bar{\omega}_1}{\partial z^2} \tag{4}$$

$$\frac{\partial \bar{\omega}_2}{\partial t} + w\frac{\partial \bar{\omega}_2}{\partial z} = \frac{\Lambda}{\rho j}\frac{\partial^2 \bar{\omega}_2}{\partial z^2} \tag{5}$$

$$\frac{\partial T}{\partial t} + w\frac{\partial T}{\partial z} = \frac{k_1}{\rho C_p}\frac{\partial^2 T}{\partial z^2} - \frac{1}{\rho C_p}\frac{\partial q_r}{\partial z} - \frac{Q_0(T_w - T_\infty)}{\rho C_p} + \frac{D_m k_T}{\rho C_p}\frac{\partial^2 C}{\partial z^2} \tag{6}$$

$$\frac{\partial C}{\partial t} + w\frac{\partial C}{\partial z} = D_m \frac{\partial^2 C}{\partial z^2} - \mathrm{Kr} * (C_w - C_\infty) \tag{7}$$

The boundary conditions are given by

$$u = v = 0, \bar{\omega}_1 = \bar{\omega}_2 = 0, T = T_\infty, C = C_\infty \ \text{ for } t \le 0 \tag{8}$$

$$u = U_r\left(1 + \frac{\varepsilon}{2}(e^{\mathrm{int}} + e^{-\mathrm{int}})\right), v = 0, \bar{\omega}_1 = -\frac{i}{2}\frac{\partial v}{\partial z},$$
$$\bar{\omega}_2 = \frac{i}{2}\frac{\partial u}{\partial z}, -k_1\frac{\partial T}{\partial z} = q_w, -D_m\frac{\partial C}{\partial z} = M_w \text{ at } z = 0$$

$$u = v = 0, \ \bar{\omega}_1 = \bar{\omega}_2 = 0,$$
$$T = T_\infty, C = C_\infty \quad \text{as} \quad z \to \infty \quad \text{for} \quad t > 0 \tag{9}$$

The velocity of the oscillatory plate [Ganapathy (1994)] from Equation (1), is given by,

$$w = -w_0 \tag{10}$$

Following Rosseland approximation (Brewster 1972), the radiative heat flux q_r is modelled as

$$q_r = -\frac{4\sigma^*}{3k^*}\frac{\partial T^4}{\partial z} \tag{11}$$

We expand T^4 in Taylor's series about T_∞ as follows:

$$T^4 = T_\infty^4 + 4T_\infty^3(T - T_\infty) + 6T_\infty^2(T - T_\infty)^2 + \ldots, \tag{12}$$

Neglecting higher powers in $(T - T_\infty)$, we have

$$T^4 \approx -3T_\infty^4 + 4T_\infty^3 T \tag{13}$$

Differentiating Equation (12) with respect to z and using Equation (13) we obtain

$$\frac{\partial q_r}{\partial z} = -\frac{16T_\infty^3\sigma^*}{3k^*}\frac{\partial^2 T}{\partial z^2} \tag{14}$$

The electron-atom collision frequency is assumed to be very high, so that Hall and ion slip currents cannot be neglected. Hence, the Hall and ion slip currents give rise to the velocity in the y-direction. When the strength of the magnetic field is very large, the generalised Ohm's law is modified to include the Hall and ion slip effect (Sutton and Sherman 1965),

$$\mathbf{J} = \sigma(\mathbf{E} + \mathbf{V} \times \mathbf{B}) - \frac{\omega_e\tau_e}{B_0}(\mathbf{J} \times \mathbf{B}) + \frac{\omega_e\tau_e\beta_i}{B_0^2}((\mathbf{J} \times \mathbf{B}) \times \mathbf{B}) \tag{15}$$

Further, the Hall parameter $\beta_e = \omega_e\tau_e \approx \mathrm{O}(1)$ and the ion slip parameter $\beta_i = \omega_i\tau_i << 1$ are taken into consideration in Equation (15), the electron pressure gradient and thermoelectric effects are neglected, i.e. the electric field $E = 0$, under these assumptions, Equation (15) is reduced to component forms as,

$$(1 + \beta_i\beta_e)J_x + \beta_e J_y = \sigma B_0 v \tag{16}$$

$$(1 + \beta_i\beta_e)J_y - \beta_e J_x = -\sigma B_0 u \tag{17}$$

On solving Equations (16) and (17) we obtain

$$J_x = \sigma B_0(\alpha_2 u + \alpha_1 v) \tag{18}$$

$$J_y = -\sigma B_0(\alpha_2 v - \alpha_1 u) \tag{19}$$

where $\alpha_1 = ((1 + \beta_e\beta_i)/(1 + \beta_e\beta_i)^2 + \beta_e^2)$ and $\alpha_2 = ((\beta_e)/(1 + \beta_e\beta_i)^2 + \beta_e^2)$

Substituting Equations (18) and (19) in (3) and (2), respectively, we get

$$\frac{\partial u}{\partial t} + w\frac{\partial u}{\partial z} - 2\Omega v = (\nu + \nu_r)\frac{\partial^2 u}{\partial z^2} + \frac{\sigma B_0^2(\alpha_2 v - \alpha_1 u)}{\rho} - \frac{\nu}{k}u + g\beta_T(T - T_\infty) + g\beta_C(C - C_\infty) - \nu_r\frac{\partial \bar{\omega}_2}{\partial z} \tag{20}$$

$$\frac{\partial v}{\partial t} + w\frac{\partial v}{\partial z} + 2\Omega u = (\nu + \nu_r)\frac{\partial^2 v}{\partial z^2} - \frac{\sigma B_0^2(\alpha_2 u + \alpha_1 v)}{\rho} - \frac{\nu}{k}v + \nu_r\frac{\partial \bar{\omega}_1}{\partial z} \tag{21}$$

Let us introduce the following non-dimensional variables:

$$u* = \frac{u}{U_r}, \ v* = \frac{v}{U_r}, \ z* = \frac{zU_r}{\nu}, \ t* = \frac{tU_r^2}{\nu}, \ n* = \frac{n\nu}{U_r^2},$$
$$\bar{\omega}_1* = \frac{\bar{\omega}_1\nu}{U_r^2}, \ \bar{\omega}_2* = \frac{\bar{\omega}_2\nu}{U_r^2}, \lambda = \frac{v_r}{v}, \ \theta = \frac{k_1(T - T_\infty)}{q_w}$$

$$\phi = \frac{D_m(C - C_\infty)}{M_w}, R = \frac{\Omega\nu}{U_r^2}, \ M = \frac{B_0}{U_r}\sqrt{\frac{\sigma\nu}{\rho}}, \ \mathrm{Pr} = \frac{\mu\rho C_p}{k_1},$$
$$\mathrm{Sc} = \frac{\nu}{D_m}, \ \mathrm{Gr} = \frac{\nu g\beta_T q_w}{k_1 U_r^3}, \ \delta = \frac{\Lambda}{\mu j}$$

$$\mathrm{Gm} = \frac{\nu g\beta_C M_w}{D_m U_r^3}, \ \mathrm{N} = \frac{4T^3\sigma^*}{k_1 k^*}, \ K = \frac{kU_r^2}{\nu^2}\mathrm{Du} = \frac{k_1^2 K_T M_w}{q_w\rho c\mu},$$
$$S = \frac{w_0}{U_r}, \ \mathrm{Kc} = \frac{\mathrm{Kr}\,\nu}{U_r^2}, \ Q = \frac{Q_0\nu^2}{U_r^2 k_1}$$

Using non-dimensional quantities, the governing equations (20), (21), (4) to (7) reduces to (Dropping asterisks)

$$\frac{\partial u}{\partial t} - S\frac{\partial u}{\partial z} - 2Rv = (1 + \lambda)\frac{\partial^2 u}{\partial z^2} + M^2(\alpha_2 v - \alpha_1 u)$$

$$-\frac{1}{K}u+\mathrm{Gr}\theta+\mathrm{Gm}\phi-\lambda\frac{\partial\bar{\omega}_2}{\partial z} \tag{22}$$

$$\frac{\partial v}{\partial t}-S\frac{\partial v}{\partial z}+2Ru=(1+\lambda)\frac{\partial^2 v}{\partial z^2}-M^2(\alpha_2 u+\alpha_1 v)-\frac{1}{K}v+\lambda\frac{\partial\bar{\omega}_1}{\partial z} \tag{23}$$

$$\frac{\partial\bar{\omega}_1}{\partial t}-S\frac{\partial\bar{\omega}_1}{\partial z}=\delta\frac{\partial^2\bar{\omega}_1}{\partial z^2} \tag{24}$$

$$\frac{\partial\bar{\omega}_2}{\partial t}-S\frac{\partial\bar{\omega}_2}{\partial z}=\delta\frac{\partial^2\bar{\omega}_2}{\partial z^2} \tag{25}$$

$$\frac{\partial\theta}{\partial t}-S\frac{\partial\theta}{\partial z}=\frac{1}{\mathrm{Pr}}\left(1+\frac{4N}{3}\right)\frac{\partial^2\theta}{\partial z^2}+\frac{Q\theta}{\mathrm{Pr}}+\mathrm{Du}\frac{\partial^2\phi}{\partial z^2} \tag{26}$$

$$\frac{\partial\phi}{\partial t}-S\frac{\partial\phi}{\partial z}=\frac{1}{\mathrm{Sc}}\frac{\partial^2\phi}{\partial z^2}-\mathrm{Kc}\,\phi \tag{27}$$

Corresponding boundary conditions are

$$u=v=0,\bar{\omega}_1=\bar{\omega}_2=0,\ \theta=0,\ \phi=0\ \text{ for } t\le 0 \tag{28}$$

$$u=1+\frac{\varepsilon}{2}(e^{\mathrm{int}}+e^{-\mathrm{int}}),v=0,\bar{\omega}_1=-\frac{i}{2}\frac{\partial v}{\partial z},\quad \bar{\omega}_2=\frac{i}{2}\frac{\partial u}{\partial z},\ \frac{\partial\theta}{\partial z}=-1,\ \frac{\partial\phi}{\partial z}=-1\quad \text{at } z=0$$

$$u=v=0,\bar{\omega}_1=\bar{\omega}_2=0,\ \theta=0,\quad \phi=0\quad \text{as}\quad z\to\infty\quad \text{for}\quad t>0 \tag{29}$$

Combining Equations (22)–(25), let $q=u+iv$ and $\omega=\bar{\omega}_1+i\bar{\omega}_2$,

$$\frac{\partial q}{\partial t}-S\frac{\partial q}{\partial z}=(1+\lambda)\frac{\partial^2 q}{\partial z^2}-\left(M^2(\alpha_1+i\alpha_2)+\frac{1}{K}+2iR\right)q+\mathrm{Gr}\theta+\mathrm{Gm}\phi+i\lambda\frac{\partial\omega}{\partial z} \tag{30}$$

$$\frac{\partial\omega}{\partial t}-S\frac{\partial\omega}{\partial z}=\delta\frac{\partial^2\omega}{\partial z^2} \tag{31}$$

Revised boundary conditions are

$$q=0,\omega=0,\ \theta=0,\ \phi=0\ \text{ for } t\le 0 \tag{32}$$

$$q=1+\frac{\varepsilon}{2}(e^{\mathrm{int}}+e^{-\mathrm{int}}),\omega=\frac{i}{2}\frac{\partial q}{\partial z},\ \frac{\partial\theta}{\partial z}=-1,\ \frac{\partial\phi}{\partial z}=-1,\quad \text{at } z=0$$

$$q=0,\omega=0,\ \theta=0,\ \phi=0\quad \text{as}\quad z\to\infty\quad \text{for}\quad t>0 \tag{33}$$

The solutions of Equations (30) and (31) and (26) and (27) under the boundary conditions (32) and (33) can be determined by the Galarkin finite element method. The steps involved in the finite-element analysis are discretisation of the domain, derivation of the element equations, assembly of elements, impositions of boundary conditions and solution of the assembled equations.

The coefficients of skin-friction, wall couple stress, Nusselt number and Sherwood number are obtained as

$$C_f=\left(\frac{\partial q}{\partial z}\right)_{z=0},\ C_w=\left(\frac{\partial\omega}{\partial z}\right)_{z=0},\ Nu=\left(\frac{\partial\theta}{\partial z}\right)_{z=0},\quad Sh=\left(\frac{\partial\phi}{\partial z}\right)_{z=0} \tag{34}$$

It is authenticated the rightness as well as validity of the arithmetical outcomes connected through the weighted residual Galerkins technique. A grids improvement investigation was carried out for separating the complete area into consecutively sized grid 91×91, 111×111 as well as 131×131 in the y-direction. Additionally the extended codes were run for dissimilar grids sized and finally it was found that each and every solution is not dependent on the grids. Following a lot of examinations it was approved that the grid sized has 111 intervals. Thus, every computation was obtained through 111 intervals of equal steps sizes of 0.01. Near each node, six variables were found as later assemble of element equations, the sets of 808 non-linearised equations were evaluated and with this might not produce the closed forms solution, subsequently iterative schemes were assumed to be solved in the systems by introducing the frontier conditions. Finally, the solutions are assumed to be convergent when the relative differentiation through two succeeding iterations was less than the quantity 10^{-8}.

3. Results and discussion

The consequences of thermo-diffusion, chemical reaction, Hall and ion-slip impacts on unsteady heat and mass transport of free convective hydro-magnetic micro-polar liquid flow enclosed past a semi-infinite porous plate within a gyratory frame under the accomplishment of a transverse magnetic field and convective boundary conditions were explored. The non-dimensional governing equations are solved systematically by means of the finite element method. The numerical calculation for the distribution of the translational velocity, micro-rotation, temperature and concentration across the boundary layer for different values of the parameters was carried out. For the purpose of our computation, we have chosen $M=K=R=\delta=N=0.5$, $\mathrm{Du}=0.5$, $Q=0.1$, $\mathrm{Kc}=1$, $\mathrm{Gr}=5$, $\mathrm{Gm}=5$, $\mathrm{Pr}=0.71$, $\lambda=0.2$, $\mathrm{Sc}=0.6$, $S=1$, $n=\pi/6$, $t=0.2$, $\beta_e=1$, $\beta_i=0.3$, the parameters are varied over a range as shown in the figures. Figures 2–18 represented the velocity, micro-rotations, temperatures and concentrations distributions, respectively. Prandtl number is a characteristic of the fluid only. For air at room temperature, Pr is 0.71 and most common gases have similar values. The Prandtl number of water at 17°C is 7.56. Liquids in general have high Prandtl numbers, with values as high as 10^5 for some oils.

The significance of Hartmann number M ahead resultant velocity and micro-rotation velocity is interpreted in Figure 2. As likely, the enlargement in M diminishes the velocity profiles. Because of the Lorentz force this emerges towards the submission by magnetic field just before an electrical conducting fluid and increases a resistive type force. Appropriate to this strength, the movement of fluid flow in momentum boundary layer thickness slows down.

From Figure 3 it can be seen that the resultant velocities increase with ever growing permeability parameter K. Apparently the larger values of K enhance the resultant velocities and consequently enlarge the momentum boundary layer thickness. Lower permeability causes lower fluid velocity which is observed

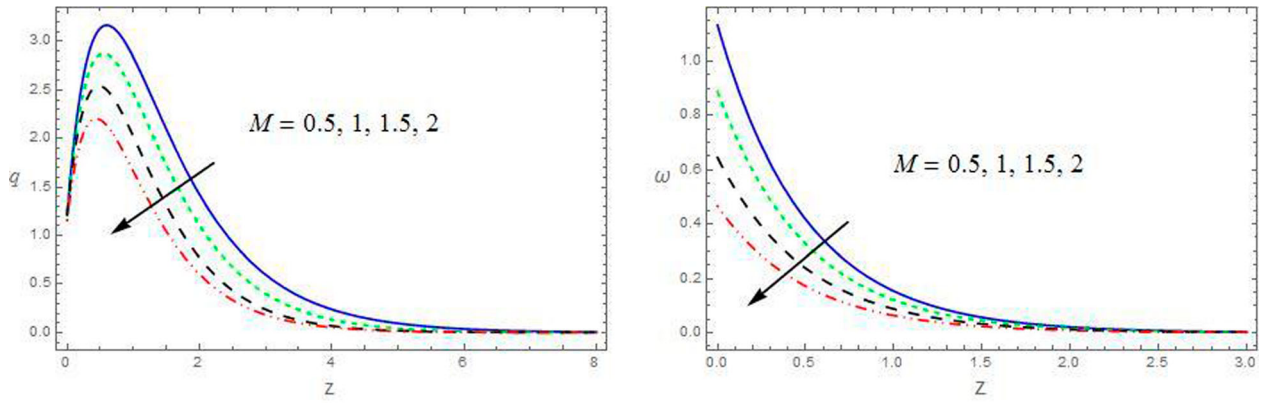

Figure 2. The velocity and micro-rotation profiles for q and ω with M.

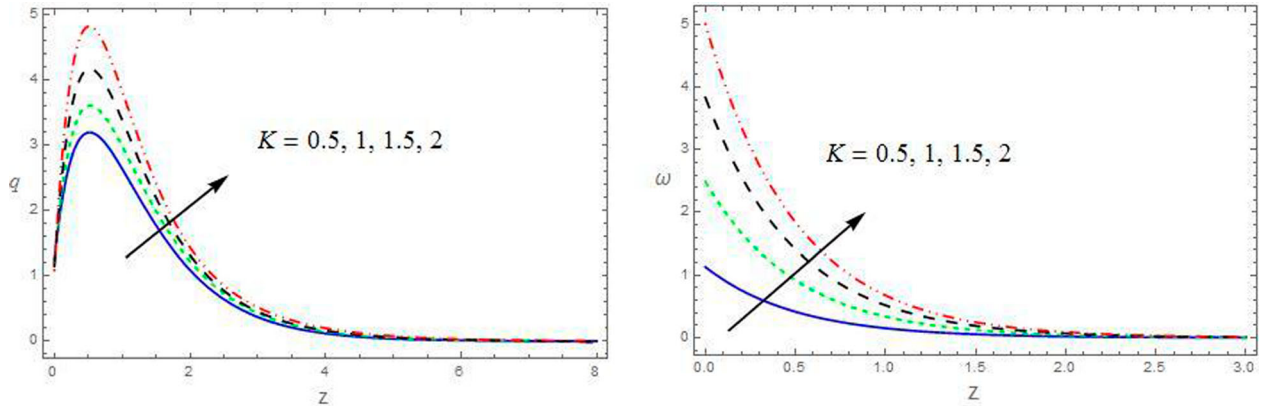

Figure 3. The velocity and micro-rotation profiles for q and ω with K.

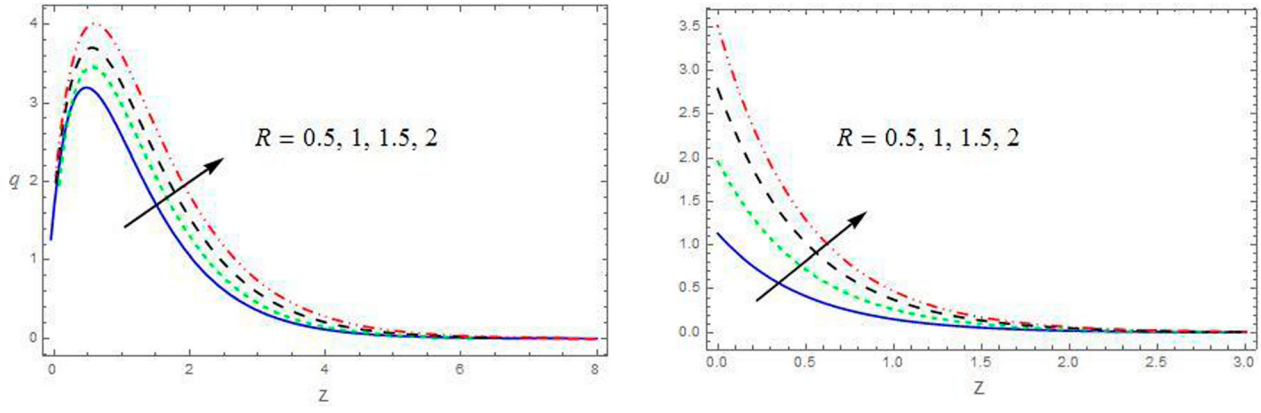

Figure 4. The velocity and micro-rotation profiles for q and ω with R.

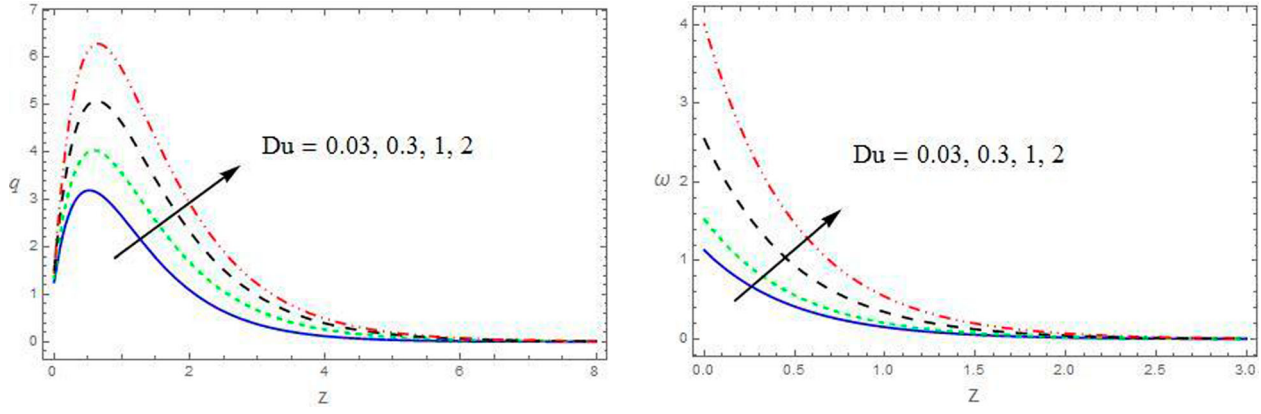

Figure 5. The velocity and micro-rotation profiles for q and ω with Du.

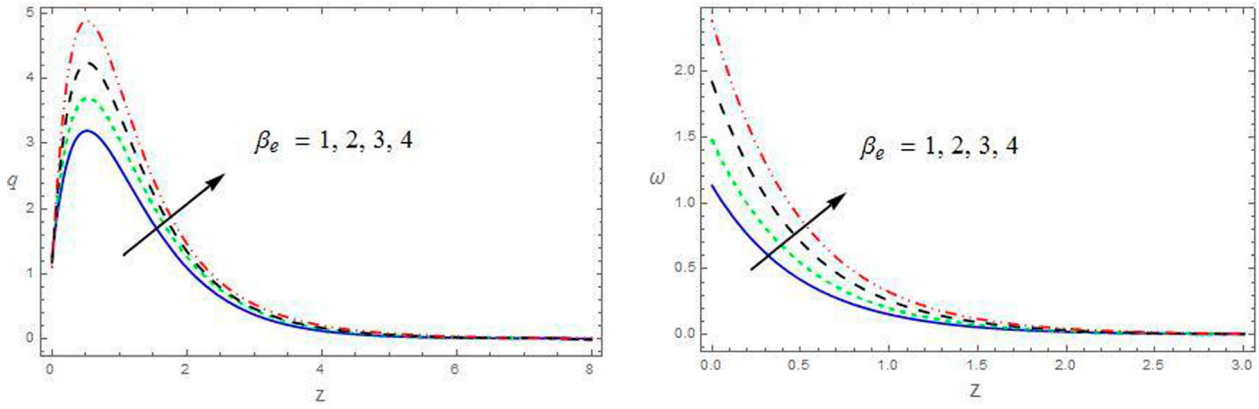

Figure 6. The velocity and micro-rotation profiles for q and ω with β_e.

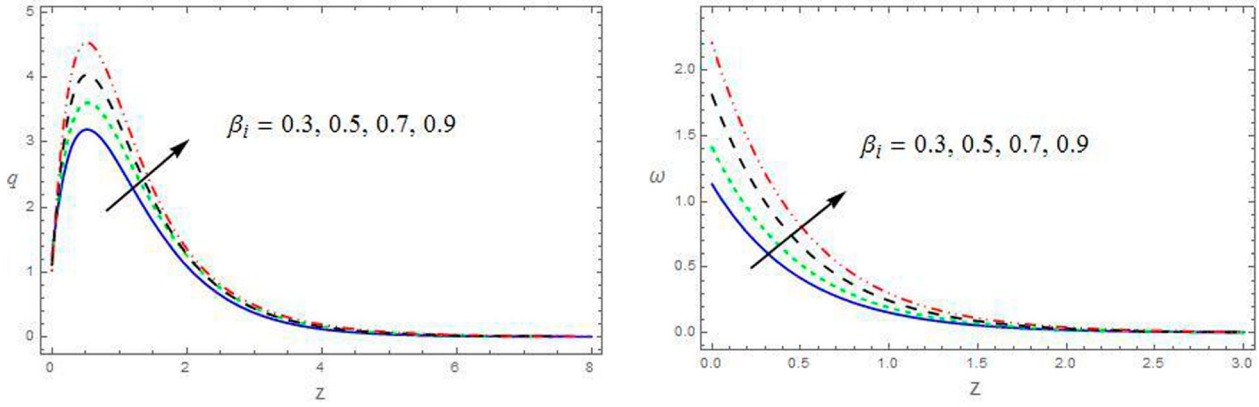

Figure 7. The velocity and micro-rotation profiles for q and ω with β_i.

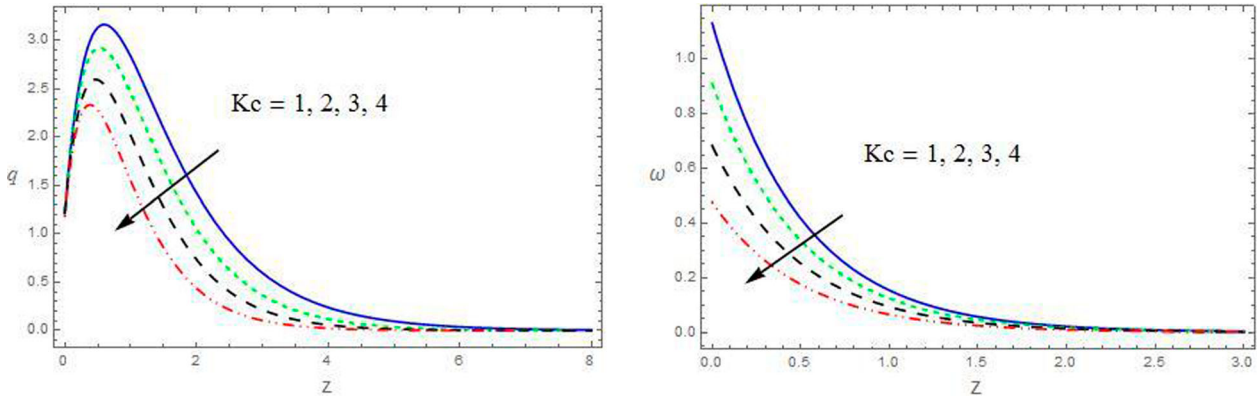

Figure 8. The velocity and micro-rotation profiles for q and ω with Kc.

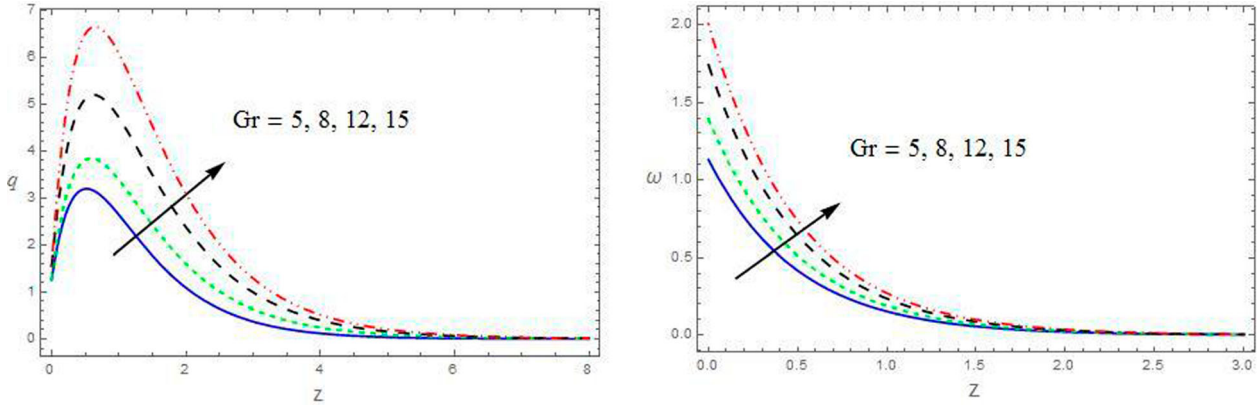

Figure 9. The velocity and micro-rotation profiles for q and ω with Gr.

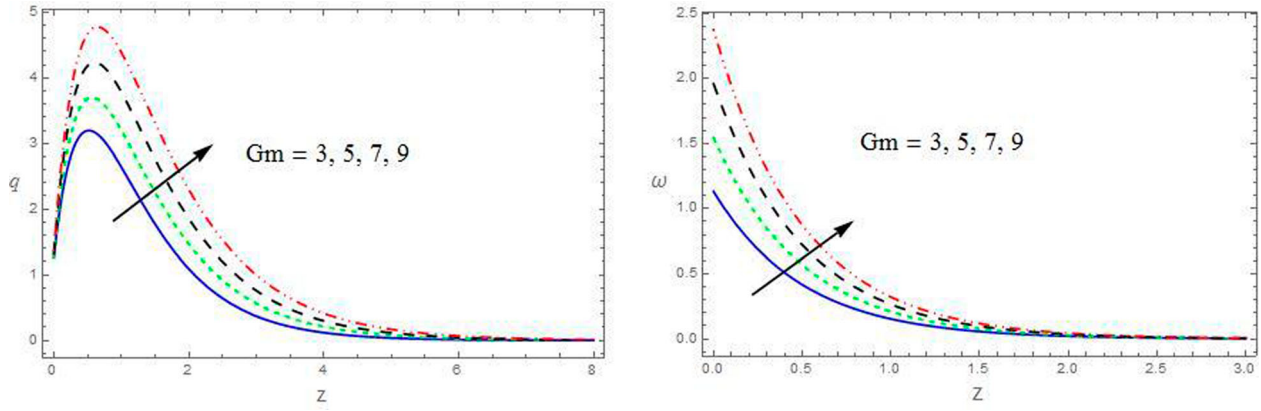

Figure 10. The velocity and micro-rotation profiles for q and ω with Gm.

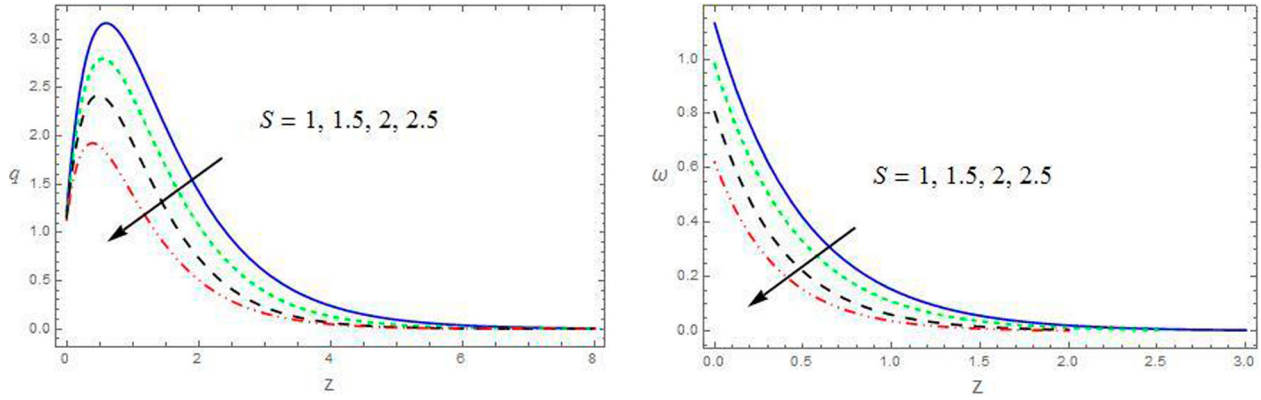

Figure 11. The velocity and micro-rotation profiles for q and ω with S.

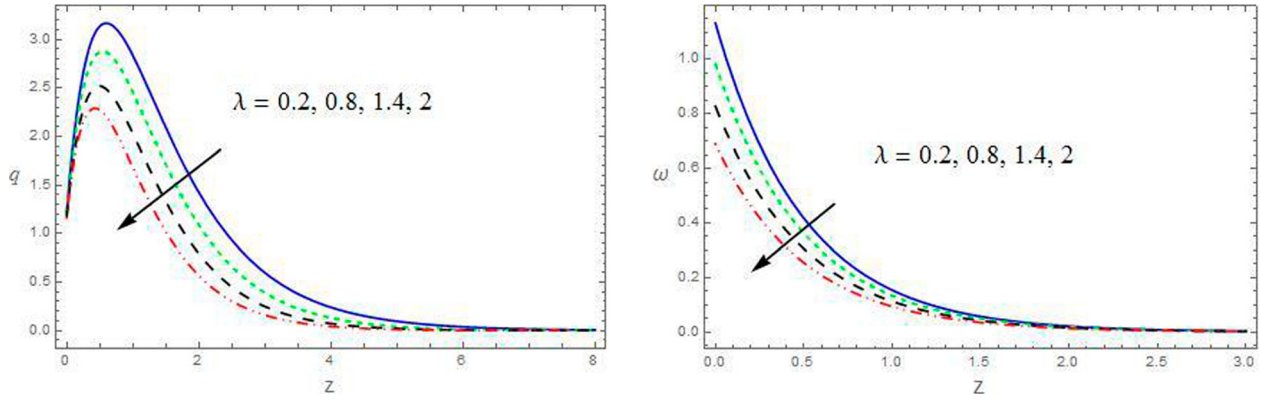

Figure 12. The velocity and micro-rotation profiles for q and ω with λ.

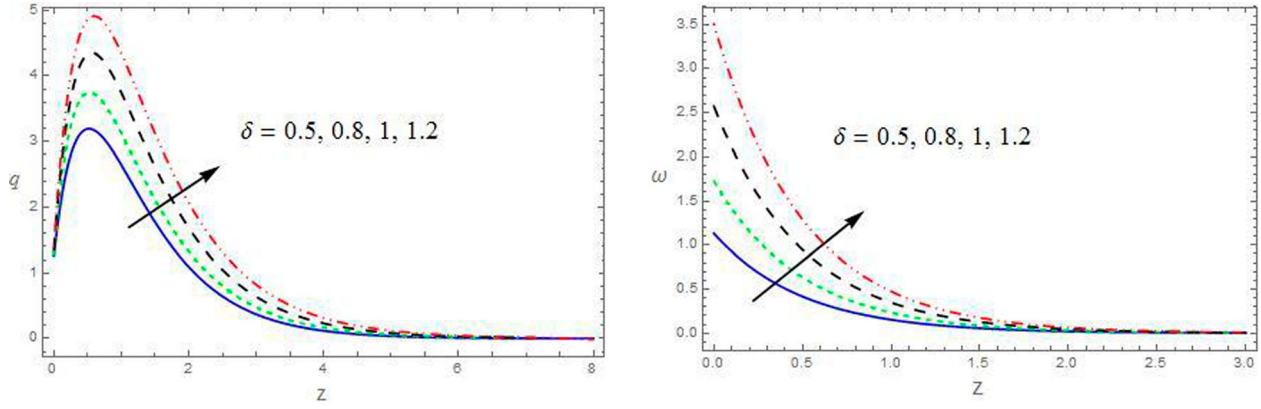

Figure 13. The velocity and micro-rotation profiles for q and ω with δ.

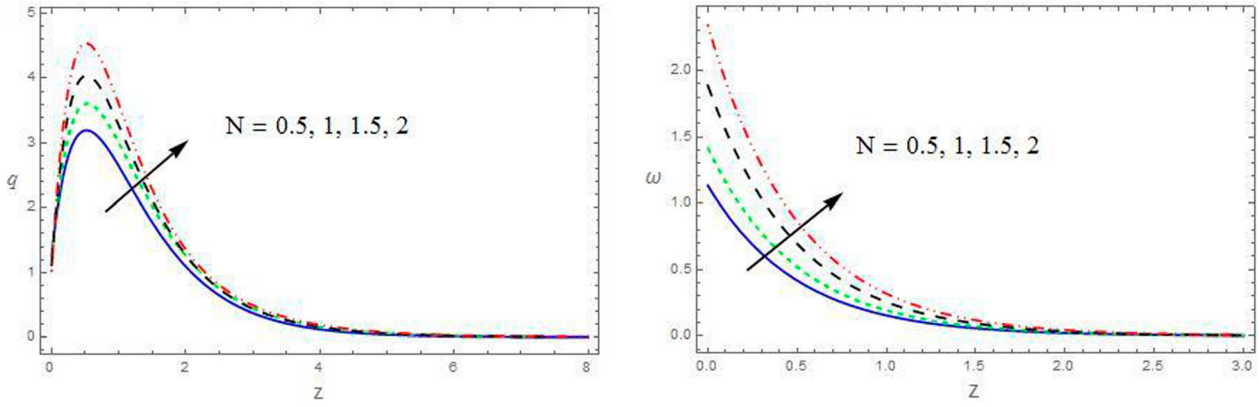

Figure 14. The velocity and micro-rotation profiles for q and ω with N.

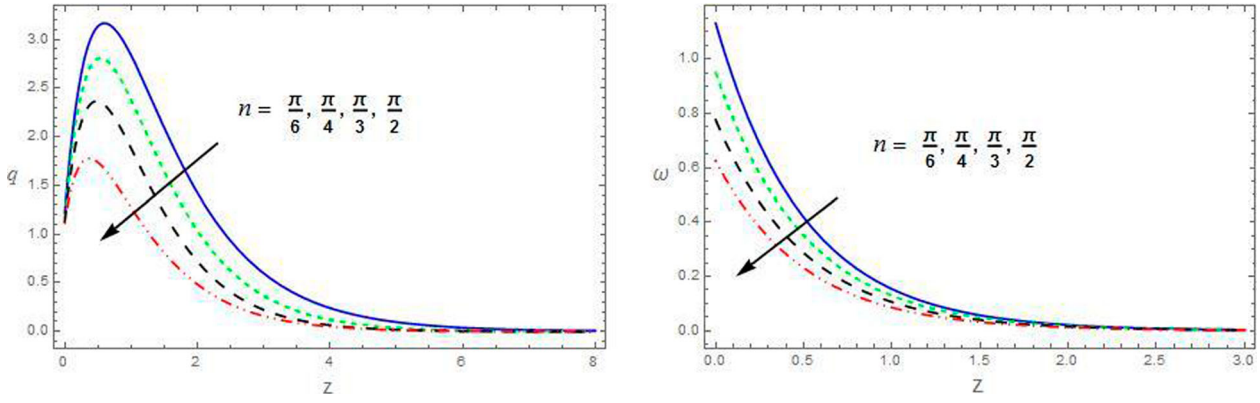

Figure 15. The velocity and micro-rotation profiles for q and ω with n.

inside flow constituency occupied by the fluid. Rotation also increases the profiles of velocity and micro-rotations in the same fashion (Figure 4). The rotation parameter has a tendency to increase both the fluid velocities all the way through the fluid region. Even though rotation is identified to persuade higher fluid velocities through the fluid region, its accelerated consequence is extensive only through the fluid area near the plate while it has good achievement on other fluid velocity through the area away from the plate. It is due to the fact that Coriolis force is overriding through the region in close proximity to the axis of rotation. Accordingly this boundary layer thickness enhances with growing rotation.

From Figure 5, it can be seen that the velocity and micro-rotation profiles boost up with increasing Dufour number. The concentration gradient results in a temperature change. Hence, an increase in the the relevant profiles.

Figures 6 and 7 depicted that the behaviour of the velocity and micro-rotation dispensations with Hall and ion-slip parameters, β_e and β_i. Reinforcement in Hall and ion-slip parameters, which results, enhances the resultant velocity, micro-rotation as well as the thickness of the momentum boundary layer all over the fluid section. The incorporation of the Hall parameter reduces the effectual conductibility and therefore decreases the magnetic renitent intensity. Also, the efficient conductivity

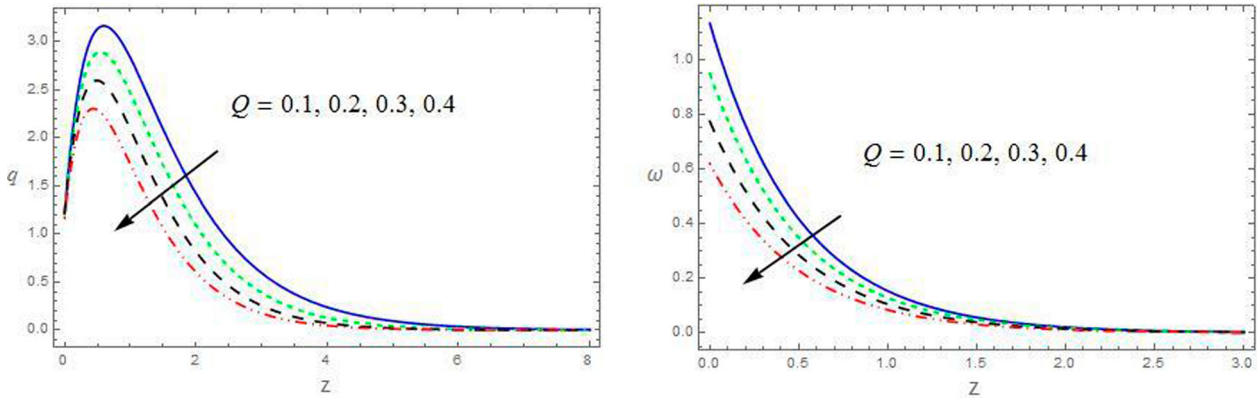

Figure 16. The velocity and micro-rotation profiles for q and ω with Q.

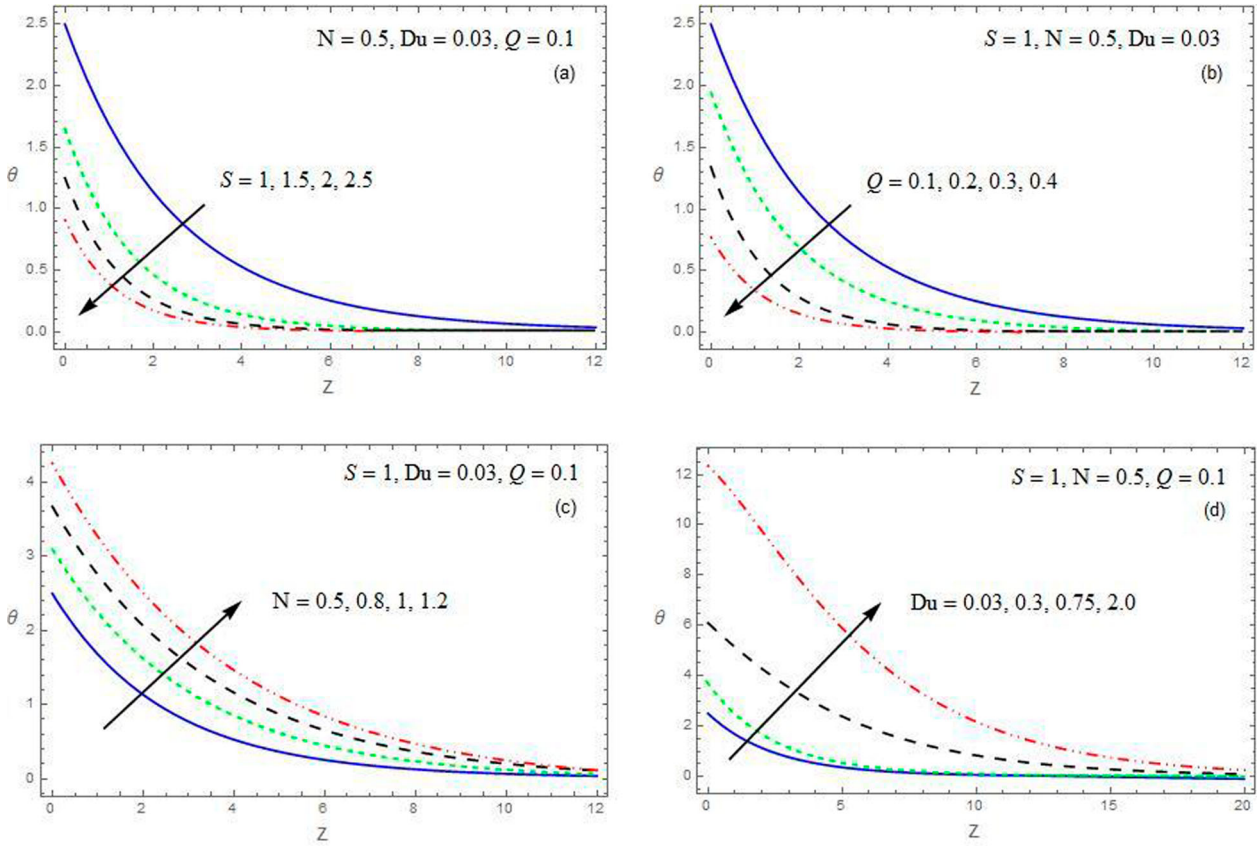

Figure 17. (a–d) the temperature profiles for θ against S, Q, N and Du.

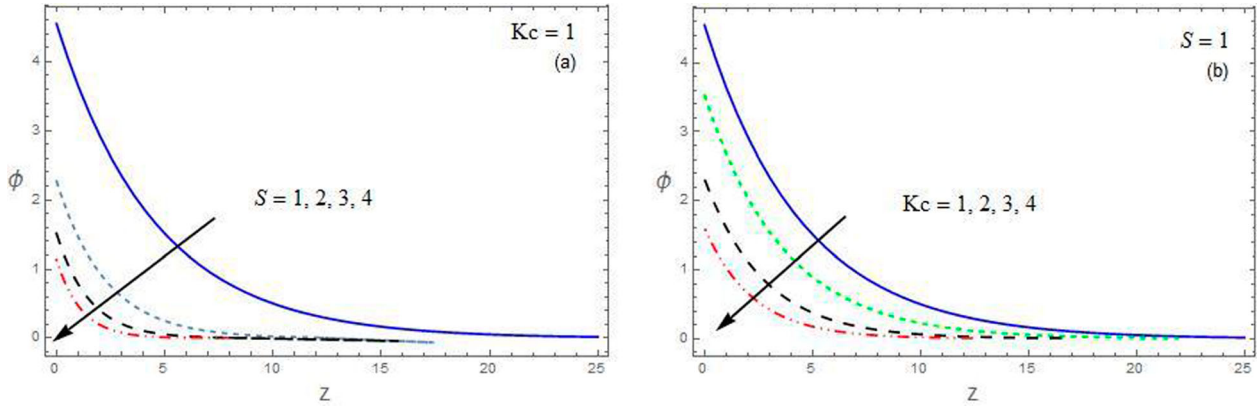

Figure 18. (a–b) the concentration profiles for ϕ against S and Kc.

causes as increase in the ion-slip parameter, and due to this the attenuation force reduces, consequently velocity increases.

We noticed that Figure 8 reveals that the velocity and micro-rotation decay with a rise in Kc. It is seen that the resultant velocity and micro-rotation decrease with an increase in the chemical reaction parameter throughout the fluid region. An increase in the chemical reaction parameter will suppress the concentration of the fluid. Higher values of chemical reaction parameter amount to a decrease in the chemical molecular diffusivity, i.e. less diffusion. Therefore, they are obtained by species transfer. Consequently, the resultant velocity and micro-rotation profiles gradually reduce.

Figures 9 and 10 depicte the special consequences of thermal and concentration buoyancy forces, the fluid velocities q and ω increase with an increase in Gr or Gm. Thermal Grashof number symbolises the comparative forces of temperature buoyancy to viscosity, likewise solutal Grashof number signifies the relative potency of concentration buoyancy force to viscous force. Hence, Gr and Gm increase with an increase in the potencies of temperature and solutal buoyancy forces accordingly. Here, the free convection flow is satisfied due to thermal and solutal buoyancy forces; hence thermal and solutal forces have a propensity to speed up the initial and secondary velocities of fluid during the boundary layer thickness in either case. It is discovered that the fluid velocities boostup nearby the surface quickly followed by grow mouldy to approaches to zero. Thus momentum boundary layer thickness increases with an enhancement in Gr or Gm.

It can be noted from Figures 11 and 12 that velocity and micro-rotation profiles trim down with increase in suction parameter S and viscosity ratio λ throughout the fluid region. Reverse trend is notified with increasing material parameter δ (Figures 13). Material parameter enhanced the momentum boundary layer throughout the fluid region.

Additionally, the consequence of thermal radiation parameter N through the both velocities profiles is shown in Figure 14. The tendency is shown that velocity augments with escalating values of the radiation parameter. It is for the reason that when the strength of the radiation parameter is enhanced this in turn boosts up the speed of heat transfer towards the fluids, the connection between the elements for the fluid particles was effortlessly wrecked furthermore it diminishes the viscosity. It would construct the fluid be in movement sooner this plays a leading role to augment of the velocity profile.

Figures 15 and 16 show the performance of velocity and micro-rotation profiles with frequency of oscillation n and heat absorption parameter Q. It is observed that velocity profiles decrease within the boundary layer with an increase in n. Similarly the velocity and micro-rotation profiles gradually reduce with increasing Q.

Figure 17(a–d) exhibits the temperature profiles with S, N, Du and Q. The temperature profiles reduce with increasing S and Q. Hence, the thickness of the thermal boundary layer retards with increasing S or Q. The opposite trend is noticed with increasing N and Du. Therefore, the thickness of the thermal boundary layer enhances.

Figure 18(a,b) signifies the concentration profiles with S and Kc. The concentration of the fluid decreases as S and Kc increase throughout the fluid region.

Table 1 depicts the effects of parameters on the skin friction coefficient C_f and couple stress coefficient C_w. It is observed that the local skin friction coefficient and couple stress coefficient increase with increasing parameters K, Du, Gr, Gm, N, β_e and β_i. The reverse effect is observed with increasing parameters M, R,

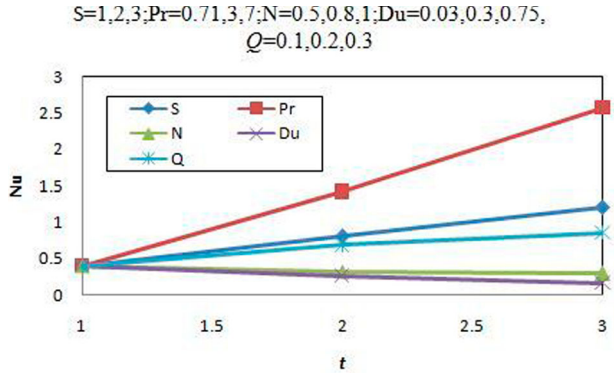

Figure 19. Nusselt number.

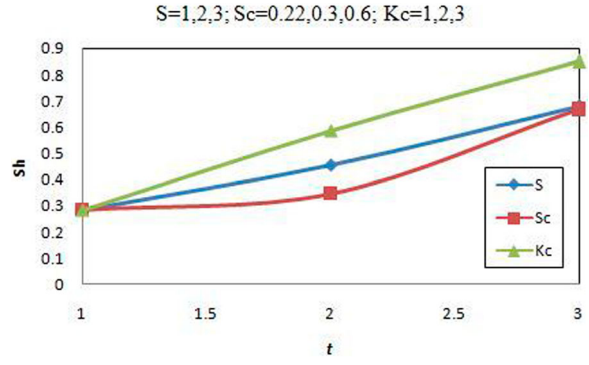

Figure 20. Sherwood number.

Table 1. Skin friction and Couple stress coefficient (Sc = 0.6, Pr = 0.71, $Q = 0.1$, $t = 0.2$).

M	R	Du	Gr	Gm	N	K	Kc	λ	δ	S	n	β_e	β_i	C_f	C_w
0.5	0.5	0.03	5	3	0.5	0.5	1	0.2	0.5	1	$\pi/6$	1	0.3	0.360704	15.2439
1.0														0.344574	13.7022
1.5														0.322987	11.7811
	1.0													0.345387	13.6405
	1.5													0.332429	12.1493
		0.3												0.487331	20.6016
		1.0												0.815630	34.4921
			8											0.468522	19.8056
			12											0.612386	25.8925
				5										0.509415	21.5359
				7										0.658162	27.8294
					1.0									0.453352	19.1639
					1.5									0.548025	23.1695
						1.0								0.403313	19.9498
						1.5								0.417904	21.9943
							2							0.214603	9.06269
							3							0198803	8.39433
								0.4						0.375556	14.2483
								0.6						0.388218	13.4120
									0.8					0.354004	9.43158
									1.0					0.350813	7.5077
										2				0.190298	12.0906
										3				0.089608	6.62875
											$\pi/4$			0.356212	15.2442
											$\pi/3$			0.349823	15.2449
												2		0.363246	15.4937
												3		0.364413	15.6093
													0.5	0.361142	15.2873
													0.7	0.361560	15.3285

Table 2. Comparison of Results for C_f and C_w ($Q = 0$, Kc $= 0$, $\beta_e = 0$, $\beta_i = 0$).

N	S	Du	R	Olajuwon and Oahimire (2013) C_f	Present C_f	Olajuwon and Oahimire (2013) C_w	Present C_w
0.5	1.0	0.03	0.5	−8.25685	−8.25684	3.25447	3.25445
1.0				−7.85547	−7.85546	3.58874	3.58871
1.5				−7.48875	−7.48874	3.78589	3.78587
	2.0			−10.2455	−10.2453	5.87499	5.87498
	3.0			−12.5585	−12.5582	7.68501	7.68499
		0.30		−6.24088	−6.24086	3.65899	3.65896
		1.00		−4.33658	−4.33656	3.74558	3.74557
			1.0	−7.68859	−7.68857	6.98554	6.98549
			1.5	−6.00145	−6.00143	9.47740	9.47739

Table 3. Comparison of Results for Nu ($Q = 0$, Kc $= 0$).

S	Pr	N	Du	Olajuwon and Oahimire (2013)	Present
1	0.71	0.5	0.03	1.025446	1.025443
2				2.335568	2.335565
3				3.699857	3.699854
	3			0.588749	0.588748
	7			0.144155	0.144153
		0.8		0.854748	0.854746
		1.0		0.699857	0.699854
			0.30	0.985547	0.985544
			0.75	0.885478	0.885476

Table 4. Comparison of results for ***Sh*** (Kc $= 0$).

S	Sc	Olajuwon and Oahimire (2013)	Present
1	0.22	0.220000	0.220000
2		0.440000	0.440000
3		0.660000	0.660000
	0.30	0.300000	0.300000
	0.60	0.600000	0.600000

$\delta$and S. The viscosity ratio increases the skin friction coefficient and reduces the couple stress coefficient. The opposite effect is observed with an increasing in n.

The Nusselt number Nu increases with increasing S, Q and Pr, while it reduces with increasing N and Du (Figure 19).

Figure 20 analyses the effect of S, Kc and Sc on Sherwood number and it was found that Sherwood number increases as S, Kc and Sc increase. These results are in good agreement with Olajuwon and Oahimire (2013) (Tables 2–4).

It is concluded that there are some advantages and disadvantages of the finite element method (FEM), which is used in this modelling. Advantages**:** The modelling of complex geometries and irregular shapes is easier as varieties of finite elements are available for the discretisation of domain. Boundary conditions can be easily incorporated in FEM. Different types of material properties can be easily accommodated in modelling from element to element or even within an element. Higher order elements may be implemented. FEM is simple, compact and result-oriented and hence widely popular among the engineering community. Availability of a large number of computer software packages and literature makes FEM a versatile and powerful numerical method. *Disadvantages*: Large amount of data are required as input for the mesh used in terms of nodal connectivity and other parameters depending on the problem. It requires a digital computer and is fairly extensive. It requires a longer execution time compared with FEM. The output result will vary considerably.

4. Conclusions

The combined effects of thermo diffusion, radiation, Hall and ion slip with suction on MHD free convection heat and mass transfer flow of an incompressible micro-polar fluid along a semi-infinite vertical permeable moving plate embedded in a porous medium in a rotating frame of reference are discussed. The significant outcomes are framed as follows. As the suction parameter increases the velocity and micro-rotation decrease, while they increase with radiating parameters, Dofour parameter, Hall along with ions slip parameters. The momentum boundary layer thickness is reduced with the escalating viscosity ratio, but the reverse effect is seen with grow in material parameter. The temperature increases with rise in Dafour parameters and radiating parameter. As the suction parameter increases, the concentration of the fluid decreases. The co-efficient of skin frictions reduces and the co-efficient of couple stress increases with rising frequency of oscillation. The Nusselts as well as Sherwoods quantities are increased with increasing suction parameter.

Disclosure statement

No potential conflict of interest was reported by the author(s).

ORCID

M. Veera Krishna http://orcid.org/0000-0002-6580-1592

References

Ahmmed, S. F., R. Biswas, and M. Afikuzzaman. 2018. "Unsteady Magnetohydrodynamic Free Convection Flow of Nanofluid through an Exponentially Accelerated Inclined Plate Embedded in a Porous Medium with Variable Thermal Conductivity in the Presence of Radiation." *Journal of Nanofluids* 7 (5): 891–901.

Bhatti, M. M., M. A. Abbas, and M. M. Rashidi. 2016. "Effect of Hall and Ion-Slip on Peristaltic Blood Flow of Eyring Powell Fluid in a Non-Uniform Porous Channel." *World Journal of Modelling and Simulation* 12 (4): 268–279.

Bhatti, M. M., S. R. Mishra, T. Abbas, and M. M. Rashidi. 2018. "A Mathematical Model of MHD Nanofluid Flow Having Gyrotactic Microorganisms with Thermal Radiation and Chemical Reaction Effects." *Neural Computing and Applications* 30: 1237–1249.

Biswas, R., M. K. Mondal, K. Shanchia, R. Ahmed, A. S. K. Samad, and S. F. Ahmmed. 2019. "Explicit Finite Difference Analysis of an Unsteady Magnetohydrodynamics Heat and Mass Transfer Micropolar Fluid Flow in the Presence of Radiation and Chemical Reaction through a Vertical Porous Plate." *Journal of Nanofluids* 8 (2): 1583–1591.

Brewster, M. Q. 1972. *Thermal Radiation Transfer Properties*. 2nd ed. New Jersey: John Wiley and Sons.

Ellahi, R., M. M. Bhatti, and I. Pop. 2016. "Effects of Hall and Ion Slip on MHD Peristaltic Flow of Jeffrey Fluid in a Non-Uniform Rectangular Duct." *International Journal of Numerical Methods for Heat & Fluid Flow* 26 (6): 1802–1820.

Erigen, A. C. 1996. "Theory of Micropolar Fluids." *Journal of Mathematics and Mechanics* 16: 1–18.
Ganapathy, R. 1994. "A Note on Oscillatory Couette Flow in a Rotating System." *Journal of Applied Mechanics* 61: 208–209.
Hari, R. K., and R. P. Harshad. 2019. "Effects of Chemical Reaction and Heat Generation/Absorption on Magnetohydrodynamic (MHD) Casson Fluid Flow Over an Exponentially Accelerated Vertical Plate Embedded in Porous Medium with Ramped Wall Temperature and Ramped Surface Concentration." *Propulsion and Power Research* 8 (1): 35–46.
Jitendra, K. S., and C. T. Srinivasa. 2018. "Unsteady Natural Convection Flow of a Rotating Fluid Past an Exponential Accelerated Vertical Plate with Hall Current, Ion-Slip and Magnetic Effect." *Multidiscipline Modeling in Materials and Structures* 14 (2): 216–235.
Krishna, M. V. 2020a. "Hall and ion Slip Effects on MHD Free Convective Rotating Flow Bounded by the Semi-Infinite Vertical Porous Surface." *Heat Transfer* 49 (4): 1920–1938.
Krishna, M. V. 2020b. "Hall and ion Slip Effects on MHD Laminar Flow of an Elastico-Viscous (Walter's-B) Fluid." *Heat Transfer* 49 (4): 2311–2329.
Krishna, M. V. 2021. "Radiation-absorption, Chemical Reaction, Hall and Ion Slip Impacts on Magnetohydrodynamic Free Convective Flow Over Semi-Infinite Moving Absorbent Surface." *Chinese Journal of Chemical Engineering*. doi: 10.1016/cjche.2020.12.026
Krishna, M. V., N. A. Ahamad, and A. F. Aljohani. 2021c. "Thermal Radiation, Chemical Reaction, Hall and Ion Slip Effects on MHD Oscillatory Rotating Flow of Micro-Polar Liquid." *Alexandria Engineering Journal* 60: 3467–3484.
Krishna, M. V., A. N. Ahamad, and A. J. Chamkha. 2020a. "Hall and Ion Slip Effects on Unsteady MHD Free Convective Rotating Flow Through a Saturated Porous Medium over an Exponential Accelerated Plate." *Alexandria Engineering Journal* 59: 565–577.
Krishna, M. V., N. A. Ahamad, and A. J. Chamkha. 2021a. "Numerical Investigation on Unsteady MHD Convective Rotating Flow Past an Infinite Vertical Moving Porous Surface." *Ain Shams Engineering Journal*. doi: 10.1016/j.asej.2020.10.013
Krishna, M. V., N. A. Ahamad, and A. J. Chamkha. 2021b. "Radiation Absorption on MHD Convective Flow of Nanofluids through Vertically Travelling Absorbent Plate." *Ain Shams Engineering Journal*. doi: 10.1016/j.asej.2020.10.028
Krishna, M. V., P. V. S. Anand, and A. J. Chamkha. 2019. "Heat and Mass Transfer on Free Convective Flow of a Micropolar Fluid through a Porous Surface with Inclined Magnetic Field and Hall Effects." *Special Topics & Reviews in Porous Media: An International Journal* 10 (3): 203–223.
Krishna, M. V., and A. J. Chamkha. 2019. "Hall and Ion Slip Effects on MHD Rotating Boundary Layer Flow of Nanofluid Past an Infinite Vertical Plate Embedded in a Porous Medium." *Results in Physics* 15: 102652.
Krishna, M. V., and A. J. Chamkha. 2020a. "Hall and Ion Slip Effects on MHD Rotating Flow of Elastico-Viscous Fluid through Porous Medium." *International Communications in Heat and Mass Transfer* 113: 104494.
Krishna, M. V., and A. J. Chamkha. 2020b. "Hall and Ion Slip Effects on Unsteady MHD Convective Rotating Flow of Nanofluids—Application in Biomedical Engineering." *Journal of the Egyptian Mathematical Society* 28 (1): 1–14.
Krishna, M. V., C. S. Sravanthi, and R. S. R. Gorla. 2020b. "Hall and Ion Slip Effects on MHD Rotating Flow of Ciliary Propulsion of Microscopic Organism through Porous Media." *International Communications in Heat and Mass Transfer* 112: 104500.
Krishna, M. V., B. V. Swarnalathamma, and A. J. Chamkha. 2018. "Heat and Mass Transfer on Magnetohydrodynamic Chemically Reacting Flow of a Micropolar Fluid through a Porous Medium with Hall Effects." *Special Topics & Reviews in Porous Media: An International Journal* 9 (4): 347–364.
Ma, Y., Mohebbi, R., M. M. Rashidi, Z. Yang, and M. A. Sheremet. 2018. "Numerical Study of MHD Nanofluid Natural Convection in a Baffled U-Shaped Enclosure." *International Journal of Heat and Mass Transfer* 130: 123–134.
Mishra, S. R., I. Khanb, Q. M. Al-Mdallac, and T. Asifad. 2018. "Free Convective Micropolar Fluid Flow and Heat Transfer over a Shrinking Sheet with Heat Source." *Case Studies in Thermal Engineering* 11: 113–119.
Olajuwon, B. I., and J. I. Oahimire. 2013. "Unsteady Free Convection Heat and Mass Transfer in an MHD Micro-Polar Fluid in the Presence of Thermo Diffusion and Thermal Radiation." *International Journal of Pure and Apllied Mathematics* 84 (2): 15–37.
Pal, D., and S. Biswas. 2018. "Magnetohydrodynamic Convective-Radiative Oscillatory Flow of a Chemically Reactive Micropolar Fluid in a Porous Medium." *Propulsion and Power Research* 7 (2): 158–170.
Pradhan, S. R., S. Baag, S. R. Mishra, and M. R. Acharya. 2019. "Free Convective MHD Micropolar Fluid Flow with Thermal Radiation and Radiation Absorption: A Numerical Study." *Heat Transfer-Asian Research* 48 (6): 2613–2628.
Rashad, A. M., Rashidi, M. M., Lorenzini, G., Ahmed, S. E., & A. M. Aly. 2017. "Magnetic Field and Internal Heat Generation Effects on the Free Convection in a Rectangular Cavity Filled with a Porous Medium Saturated with Cu–Water Nanofluid." *International Journal of Heat and Mass Transfer* 104: 878–889.
Rashidi, M. M., P. A. Mohimanian, and S. Abbasbandy. 2011. "Analytic Approximate Solutions for Heat Transfer of a Micropolar Fluid Through a Porous Medium with Radiation." *Communications in non-Linear Science and Numerical Simulation* 16: 1874–1889.
Sara, I. A., and M. M. Bhatti. 2018. "The Study of Non-Newtonian Nanofluid with Hall and Ion Slip Effects on Peristaltically Induced Motion in a Non-Uniform Channel." *RSC Advances* 8: 7904–7915.
Sobamowo, M. G. 2018. "Combined Effects of Thermal Radiation and Nanoparticles on Free Convection Flow and Heat Transfer of Casson Fluid Over a Vertical Plate." *International Journal of Chemical Engineering* 2018: 1–25.
Srinivas, S., C. K. Kumar, and A. S. Reddy. 2018. "Pulsating Flow of Casson Fluid in a Porous Channel with Thermal Radiation, Chemical Reaction and Applied Magnetic Field." *Nonlinear Analysis: Modelling and Control* 23 (2): 213–233.
Srinivasacharya, D., and Md. Shafeeurrahman. 2017. "Hall and ion Slip Effects on Mixed Convection Flow of Nanofluid between Two Concentric Cylinders." *Journal of the Association of Arab Universities for Basic and Applied Sciences* 24 (1): 223–231.
Sutton, G., and A. Sherman. 1965. *Engineering Magnetohydrodynamics*. New York: Mc Graw Hill.
Ziaul Haque, Md, Md. Mahmud Alam, M. Ferdows, and A. Postelnicu. 2012. "Micropolar Fluid Behaviors on Steady MHD Free Convection and Mass Transfer Flow with Constant Heat and Mass Fluxes, Joule Heating and Viscous Dissipation." *Journal of King Saud University – Engineering Sciences* 24: 71–84.